IEEE Access
Multidisciplinary | Rapid Review | Open Access Journal

Received June 28, 2019, accepted July 20, 2019, date of publication August 2, 2019, date of current version August 16, 2019.

Digital Object Identifier 10.1109/ACCESS.2019.2932912

Parametric Study of 3D Additive Printing Parameters Using Conductive Filaments on Microwave Topologies

FRANCISCO PIZARRO[1], (Member, IEEE), ROLANDO SALAZAR[1], EVA RAJO-IGLESIAS[2], (Senior Member, IEEE), MAURICIO RODRÍGUEZ[1], (Senior Member, IEEE), SEBASTIAN FINGERHUTH[1], (Member, IEEE), AND GABRIEL HERMOSILLA[1]

[1]Escuela de Ingenieria Eléctrica, Pontificia Universidad Católica de Valparaíso, Valparaíso 2147, Chile
[2]Department of Signal Theory and Communication, University Carlos III of Madrid, 28911 Madrid, Spain

Corresponding author: Francisco Pizarro (francisco.pizarro.t@pucv.cl)

This work was supported in part by the FONDECYT INICIACION under Grant 11180434 and Grant 1150388, PCI MEC80180108, Proyecto VRIEA-PUCV 039.462/2017, and in part by the Spanish Government under Project TEC2016-79700-C2-2-R.

ABSTRACT This paper presents a parametric study of classical additive 3D-printing settings for use on conductive filaments in applications for high-frequency topologies. First, a wideband characterization was conducted, printing a microstrip transmission line using a conductive filament with variations of typical 3D-printing settings, such as layer height, infill percentage, and infill pattern. The measurement results show a dependence on the high-frequency transmission parameters with respect to the infill percentage and the infill pattern. Finally, two antennas were 3D-printed using conductive material, a microstrip patch, and a low-weight pyramidal horn antenna. The results for the patch agree with the losses found on the line measurements, while the low-weight pyramidal horn exhibits no major differences compared with its equivalent antenna, made using perfect conductors.

INDEX TERMS 3D-printing, wideband characterization, 3D-printed antennas, conductive PLA.

I. INTRODUCTION

Currently, 3D-printing has changed the methods of manufacturing and prototyping. The precision of new-generation printers, in addition to the variety of materials, has made possible the construction of structures and models that previously were too difficult or expensive to build [1]–[4]. 3D-printing techniques vary depending on the materials, accuracy and costs addressed by the manufacturer. Techniques such as additive 3D printing, deposition and laser are the most used, where the choice among them depends on the materials, the required precision and the overall cost.

One of the issues that involves the realization of a high-frequency topology such as an antenna is that some specifications cannot be found on the market, either because of its shape, size, resonance frequency or bandwidth, creating the need for the design and construction of prototypes. Depending on the structure, these prototypes can increase the cost of the overall project and, in many cases, are time-consuming in terms of the manufacturing process. The easy-access to low-cost 3D printers can have a direct impact on the reduction of costs and time for a final high-frequency product [5]–[7]. In particular, additive 3D printing is an emerging technology that offers great potential for the manufacturing of low-cost, low-weight compact structural components for wireless applications and mobile communication systems that are also respectful to the environment.

In previous works, various additive manufacturing techniques have been implemented, such as stereolithography or 3D printing with a subsequent metallization process for the fabrication of high-frequency devices [8]–[18]. The aforementioned techniques have facilitated the rapid manufacturing of prototype antennas, showing good performances in terms of radiation characteristics [11], [19], [20]. However, there are few studies on 3D printing directly with conductive materials [21]–[24], but most of them focus

The associate editor coordinating the review of this manuscript and approving it for publication was Kwok L. Chung.

on the use of 3D-printed dielectric filaments [25], for example, in lens applications [26], [27]. The new low-cost PLA filaments available on the market with conductive characteristics [28]–[30] open the possibility for electronics applications, whether creating tracks on printed plates, filters, antennas or other high-frequency devices. Nevertheless, it is important to characterize the behavior of these new filaments for their use in higher-frequency devices in terms of different printing possibilities and to compare their behavior with that of traditional metallized structures. It is important to note that standard polylactic acid (PLA) can also be used as a substrate for high-frequency structures from the perspective of a complete fabrication of both dielectric and metallic parts in 3D printing. Therefore, it is important to also characterize the permittivity behavior of the PLA; several studies have been done under this scope [31]–[34].

To date, few studies have addressed the characterization of these new conductive filaments as a function of the frequency [21], and no studies have been carried out to characterize the performance of these filaments with respect to the printing specifications. Depending on the specific software used and the printer, each prototype can be constructed in many different ways in terms of percentage of infill, wall size, and height of the layer and infill pattern. Under this perspective, the objective of this article is to perform a wideband parametric study, using a microstrip transmission line, of the behavior of 3D printing for different printing parameters such as infill quantity, infill pattern and layer height and, finally, the use of these results for the construction of two types of antennas.

The article is divided as follows. In Section II, the materials used for the 3D printing and the 3D printer itself, including the parameters that will be studied, are introduced. In Section III, the wideband characterization of the material using a microstrip transmission line is presented, and in Section IV, two antenna applications are presented using the previously characterized material.

II. FILAMENT AND PRINTER CHARACTERISTICS

To perform a wideband parametric study, it is important to know the parameters of the materials that will be used and the printer characteristics. Currently, there are several commercial options for conductive filaments compatible with standard 3D printers. Among these possibilities, the chosen filament was the 1.75-mm Electrifi conductive filament [28]. This filament has a resistivity of 0.006 Ω·cm, one of the highest conductivities available on the market [28]. The suggested printing temperature for this filament is between 140 and 160°C, and the suggested printing speed is between 14 and 45 mm/s.

The characterization of the conductive filament will be done using a standard microstrip transmission line. Therefore, there is the need for a substrate that holds the conductive filament. To do a full integration in 3D printing, a standard 1.75-mm PLA from the manufacturer Sakata 3D [35] will be used. As this filament will be used as a

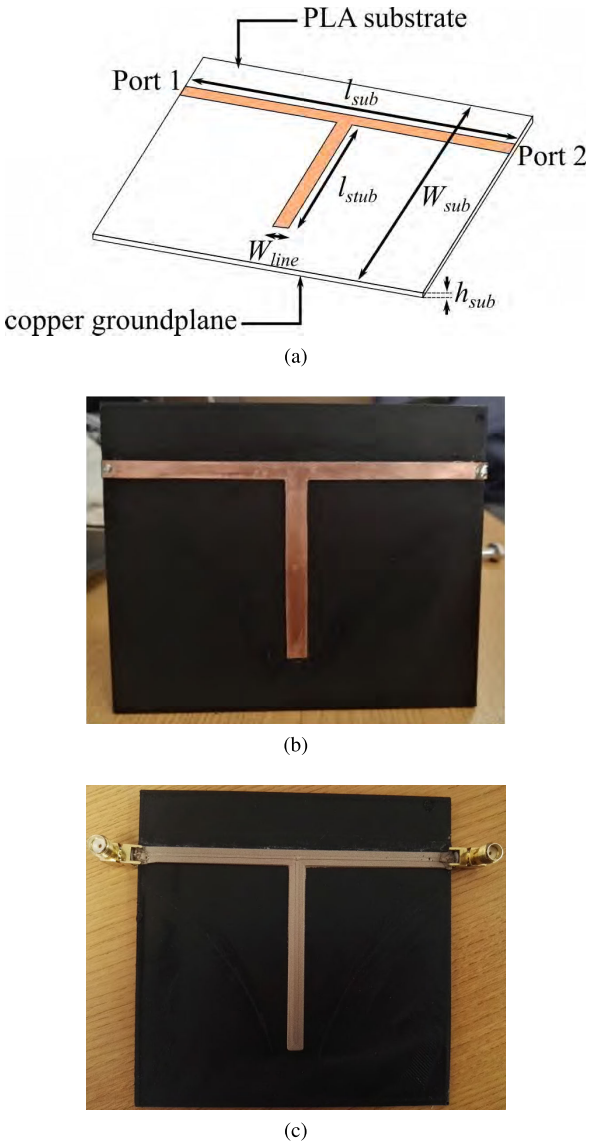

FIGURE 1. Quarter-wavelength microstrip open stub resonator. a) Isometric layout. b) Top view of the constructed resonator with copper foils. c) Top view of the constructed resonator with conductive PLA.

substrate, it is necessary to characterize it in terms of its relative permittivity ε_r. For this characterization, the method proposed in [36], [37] was used, consisting of the use of a quarter-wavelength microstrip open stub resonator to estimate the effective dielectric constant ε_{eff} of the substrate, using the central frequency and the bandwidth of the resonator (Q-factor). First, we calculate the ε_{eff} using the following equation [36]:

$$\varepsilon_{eff} = \left(\frac{n \cdot c}{4 \cdot f_0 \cdot l_{stub}}\right)^2, \quad n = 1, 3, 5 \ldots \tag{1}$$

where c is the speed of light in free space, l_{stub} is the length of the stub and f_0 is the central frequency of the resonator. Finally, to obtain the relative permittivity ε_r, classical microstrip design equations are used [38].

In Fig. 1, the constructed quarter-wavelength open stub resonator is shown. In Fig. 1a, the layout of the resonator is

described, while in Fig. 1b, the top view of the constructed device is shown. Copper foils were used for the metallic parts of the resonator (microstrip line and ground plane). The final dimensions of the resonator are the following: $h_{sub} = 1.7$ mm, $l_{sub} = W_{sub} = 100$ mm, $W_{line} = 4.5$ mm and $l_{stub} = 58.5$ mm. In addition, and in order to obtain the effective permittivity of a structure involving the PLA plus the conductive filament, another resonator was build using conductive filament (Fig. 1c). In this case, the height of the microstrip line constructed with the filament was of 1 mm.

The measured transmission coefficient $|S_{21}|$ of the quarter-wavelength open stub resonator is included in Fig. 2. The results show two resonant frequencies of the stub at 900 MHz and at 2.7 GHz. From this measurement and according to Eq. 1, the effective permittivity is approximately $\varepsilon_{eff} \approx 2.07$, which implies a relative permittivity $\varepsilon_r \approx 2.5$ of the PLA printed substrate. Using the same procedure for the resonator constructed with the PLA, we can observe a shift on the resonant frequency, which implies an overall effective permittivity (PLA+conductive PLA) of approximately $\varepsilon_{eff} \approx 1.84$ for the first resonance and for the second resonance a $\varepsilon_{eff} \approx 2.01$. We can observe that the conductive filament, which have other dielectric materials in order to make it suitable for 3D printing, has an influence on the effective permittivity of the printed structure. Also there is a frequency dependence of this parameter on the material.

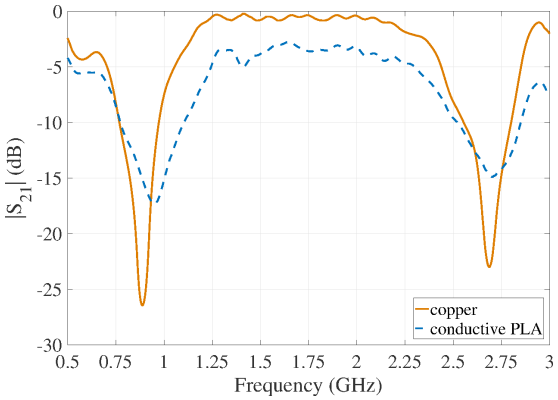

FIGURE 2. Measured $|S_{21}|$ of the quarter-wavelength open stub resonator.

To print the conductive filament, it is necessary to set the 3D printer with the specific parameters for a correct deposition. The 3D printer used in this study is an Ocular 3D [39] custom-made 3D printer that can be seen in Fig. 4. Some of the important technical parameters of the printer are presented in Table 1. The parameters of the printer were set to meet the requirements for printing the Electrifi conductive filament. To achieve better printing of the filament, the hot-end of the printer was modified with a CNC machine to guarantee better filament flux during the printing process, avoiding the damages that can be produced by the filament getting stuck in this part of the printer. The modification

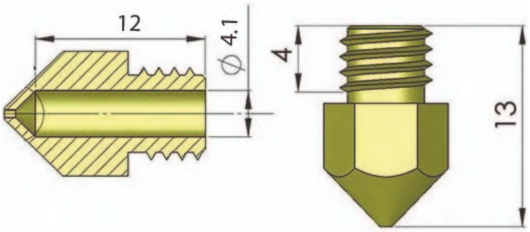

FIGURE 3. Diagram of the modified hot-end with a CNC machine (units in mm).

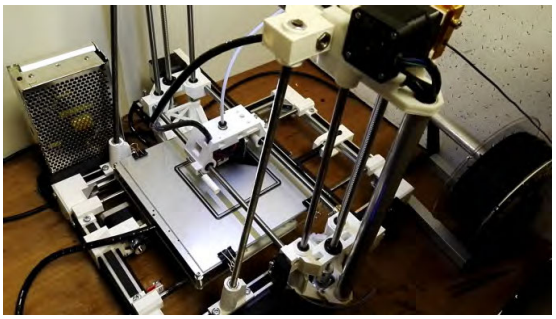

FIGURE 4. Custom-made EIE 3D printer from Ocular 3D.

TABLE 1. Ocular 3D EIE custom 3D printer technical specifications.

Printer parameter	Value
Maximum printing volume	190×190×190 mm^3
Axis resolution	100 μm in all axis *(xyz)*
Hot-end model	CNC modified E3DV6 [40]
Hot-end T° range	120 to 250°C
Platform maximum T°	75°C

consisted on modifying the inner diameter of the hot-end and heatbreak, drilling a hole to fit a teflon tube of 4.1 mm of outer radius and 2 mm of inner radius.

The wideband characterization will be done using a microstrip transmission line printed with the Electrifi conductive filament, varying the infill percentage, the layer height and the infill pattern. Therefore, the printer setup used for the correct deposition of the filament is shown in Table 2. These parameters can be set with a standard 3D-printer software, such as Ultimaker CURA [41].

TABLE 2. 3D-printer settings for conductive filament.

Printing setting	Value
Layer height	0.2, 0.25 and 0.3 mm
Infill percentage	10%, 50% and 100%
Infill pattern	concentric, triangle and zig-zag
Printing temperature	160°C
Printing speed	20 mm/s
Cooling fan	100%
Cooling time per layer	5 seconds

III. MICROSTRIP LINE CHARACTERIZATION

The effects of the various printing settings are studied through a wideband characterization using a 3D-printed

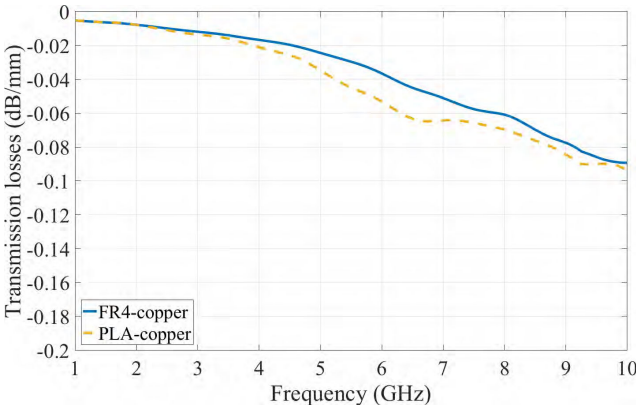

FIGURE 5. Measured transmission losses of the reference transmission line over the PLA and compared with a standard microstrip line etched on FR-4.

(a) (b)

FIGURE 6. Constructed microstrip lines. a) 3D-Printed substrate with copper foil. b) FR-4 substrate with etched copper line.

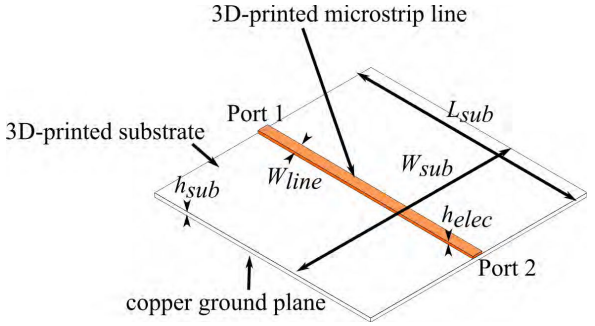

(a)

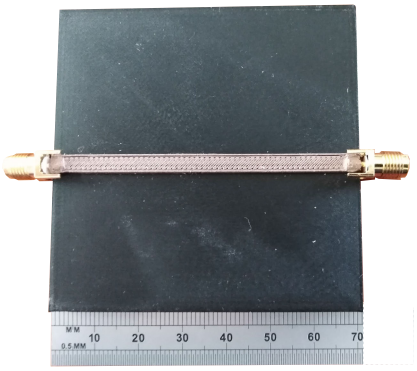

(b)

FIGURE 7. 3D-printed microstrip line. a) Isometric layout b) Top view of the constructed microstrip line.

microstrip line. Parameters such as infill percentage, infill pattern and layer height were studied with respect to their influence on the transmission losses of the transmission line. Before the characterization of the 3D-printed microstrip lines, a reference 50 Ω microstrip line is made with copper foils over the previously characterized PLA. The dimensions of the printed PLA substrate are 70 mm × 70 mm × 1.7 mm. Fig. 5 shows the transmission losses (in dB/mm) of the transmission line over the PLA substrate, compared with a traditional 50 Ω microstrip line etched on a FR-4 substrate ($\varepsilon_r = 4.4$, $\tan\delta = 0.02$) and Fig. 6 shows the constructed microstrip lines. From these results we can see that the losses introduced by the PLA substrate are comparable with a traditional FR-4 substrate. The PLA microstrip line with copper foils will be used as a reference line in terms of the dielectric losses introduced by the PLA substrate (as we assume that the losses due to the copper foils are negligible), in order to analyze only the losses introduced by the conductive filament on the microstrip line.

A. 3D-PRINTED MICROSTRIP LINE CHARACTERISTICS

Fig. 7 contains the constructed microstrip line template that will be used for the characterization. Fig. 7a shows an isometric view of the layout of the printed microstrip line. The transmission line is printed over the previously characterized PLA substrate of height $h_{sub} = 1.7$ mm and lateral dimensions of $L_{sub} = W_{sub} = 70$ mm. The Electrifi conductive line is printed with a height of $h_{elec} = 1$ mm and $W_{line} = 4.5$ mm. Finally, the ground plane is made with a copper foil and two 50 Ω SMA connectors (one on each side of the line), soldered using the same conductive filament as the microstrip line. A top view of the constructed 3D-printed microstrip line is shown in Fig. 7b. To compare the measurements and to remove the dielectric losses introduced by the substrate, the transmission losses of the copper microstrip line etched on the same PLA substrate was subtracted from the measurements results of the fully 3D microstrip line transmission coefficient.

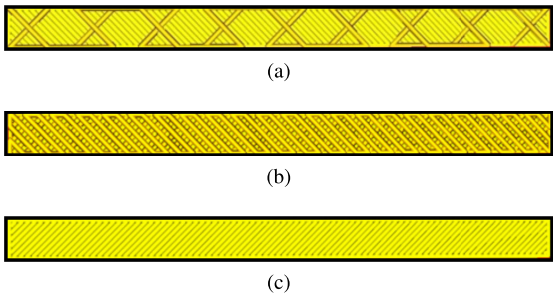

(a)

(b)

(c)

FIGURE 8. Different infill percentages for the microstrip line. a) 10% infill. b) 50% infill. c) 100% infill.

Once the microstrip line dimensions were defined, the printer settings for the study were set. First, and as shown in Fig. 8, three variations of the infill percentage were defined: 10% (Fig. 8a), 50% (Fig 8b) and 100% (Fig. 8c).

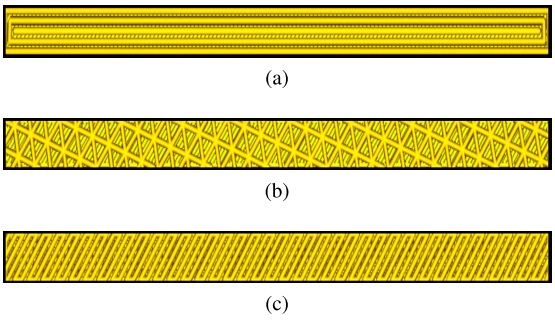

FIGURE 9. Different infill patterns used for the study. a) Concentric. b) Triangle. c) Zig-zag.

For each infill percentage, three infill pattern variations were studied: concentric infill, triangle infill and zig-zag infill. The patterns are defined in Fig. 9. Finally, the lines will be constructed using the various infill percentages and infill patterns with three different layer heights: 0.2 mm, 0.25 mm and 0.3 mm. This heights were chosen because of its stability during the printing process. Tests done with lower layer heights (i.e. 0.1 mm layers) shows poor stability in their dimensions during the printing process. In total, the combination of these parameters leads to the construction of 27 different 3D-printed microstrip lines.

B. MEASUREMENT RESULTS

The scattering parameters of the 27 3D-printed microstrip lines were measured using a Rohde & Schwarz ZVA40 Vector Network Analyzer (VNA) on a band from 1 to 10 GHz. The measurement results in terms of transmission losses (in dB/mm) for all the constructed lines are presented in Fig. 10. For a better analysis, the results are shown with respect to infill percentage. That is, Fig. 10a corresponds to the 10% infill percentage lines with the combination of different layer heights and different infill patterns, and the same is true for the 50% infill percentage (Fig. 10b) and 100% infill percentage (Fig. 10c). Note that in all the represented measurements, the reference copper line case is subtracted to neglect the dielectric losses introduced by the PLA substrate. Additionally, for all measurements, the reflection coefficient $|S_{11}|$ had values below -10 dB over the whole band.

From Fig. 10, we can see that if we increase the infill percentage, the losses tends to be lower at higher frequencies, while in the lower part of the band (below 4 GHz), there were no significant differences between the different infill percentages. Another important result is that the difference between the infill patterns becomes more relevant, while the infill percentages are lower. For example, if we consider Fig. 10a, we can see that in the higher part of the band (above 5 GHz), the losses difference between each infill pattern become more significant, with values that can differ up to 7 dB between two different patterns. This result can be explained because at lower infill percentages, the infill pattern becomes more noticeable than at higher infill percentages, when it tends to become a more uniform infill. Finally, concerning the layer height, there is a slight tendency in all cases in which the

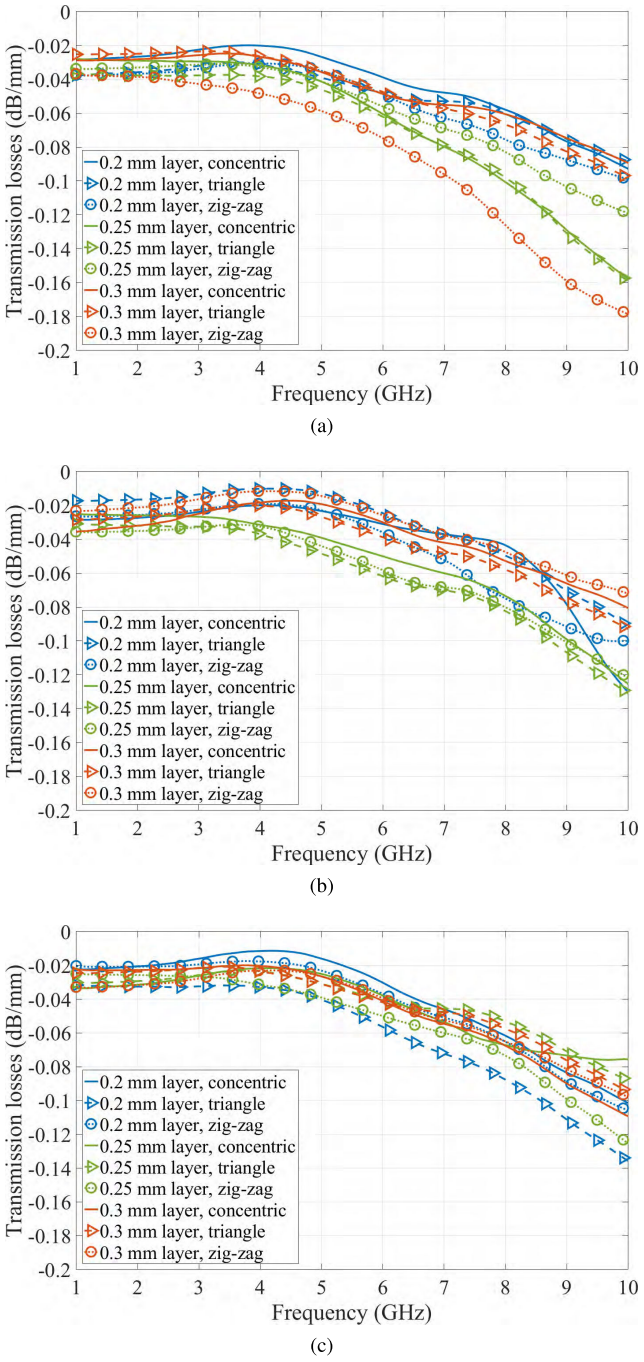

FIGURE 10. Transmission losses difference with respect copper line for different infill percentage as function of layer height and infill pattern. a) 10% infill. b) 50% infill. c) 100% infill.

0.2-mm layer has the lowest losses on average. Nevertheless, and as explained before, while increasing the infill percentage, the difference between the infill pattern and the height layer becomes less significant for most of the cases.

IV. EVALUATION ON ANTENNA APPLICATION

With the results obtained with the characterization, we constructed two different antenna topologies: a microstrip patch

antenna and a pyramidal horn antenna. First, the microstrip patch antenna was made to compare a simulated result using the manufacturer specifications for the filament with a measured one. This is an important topology to asses to establish the relationship between the measured losses in the filament for a resonant type topology and its impact on the radiation pattern.

On the other hand, the pyramidal horn antenna was made to assess two different parameters: first, to test an aperture antenna topology with a waveguide feed and, then, to evaluate the impact on the radiation parameters of reducing to a minimum the weight of the antenna using the lower quantity of filament possible for its fabrication. Both antenna radiation patterns were measured in an anechoic chamber.

A. 3D-PRINTED PATCH ANTENNA

The 3D-printed microstrip patch is presented in Fig. 11. This patch was designed for a resonance frequency f_0 of 2.5 GHz. The substrate used for the antenna was the same PLA used on the microstrip line characterization. In terms of the permittivity, the value used for this design was a $\varepsilon_{eff} = 2.01$ ($\varepsilon_r \approx 2.41$) and $h_{sub} = 1.7$ mm, which corresponds to the characterized value obtained with the quarter-wavelength open stub resonator printed with the conductive filament at the antenna frequency band. In addition a $\tan\delta = 0.02$ was used for the PLA dielectric losses, in agreement to the measured shown results in Fig. 6. The isometric layout of the printed patch antenna is shown in Fig. 11a. The final dimensions for this antenna were $W_{sub} = L_{sub} = 100$ mm, $L_{patch} = 36.95$ mm, $W_{patch} = 45.45$ mm, $L_{ins} = 10$ mm, $W_{ins} = 2$ mm and $h_{elec} = 1$ mm. In Fig. 11b, a top view of the constructed patch is shown. As previously mentioned, the 50 Ω SMA connector was soldered to the feeding microstrip line using the same Electrifi conductive filament. Finally, the antenna was constructed using 100% infill, 0.2 mm of layer height and a concentric infill pattern.

The first assessed parameter was the reflection coefficient $|S_{11}|$ of the 3D-printed antenna. The results are shown in Fig. 12. The antenna was simulated using ANSYS HFSS software and using the conductivity parameters for the filament given by the manufacturer. As a result, the measured $|S_{11}|$ of the constructed antenna gives a resonance frequency $f_0 \approx 2.5$ GHz, which matches the results obtained with simulation. Note that both cases (simulation and measurement) are well matched at the resonant frequency.

Another parameter of the antenna that was measured was its gain radiation pattern. These results are also compared with two reference antennas, one etched in FR-4 and another done with the same PLA substrate and copper foils, with its central frequency also at 2.5 GHz (Fig. 13). Both reference antennas have the same feeding topology and are constructed on a substrate with the same dimensions as the fully 3D-printed antenna ($W_{sub} = L_{sub} = 100$ mm, $h_{sub} = 1.7$ mm).

The results for the simulated and measured gains are illustrated in Fig. 14. We can see that in both planes (Fig. 14a for the E-Plane and Fig. 14b for the H-plane), a good agreement between the simulated and measured results was found in terms of the radiated mode of the patch. However, the values of the maximum gain differ in both cases. For the HFSS simulation using PLA substrate and the conductive filament, the maximum gain obtained was 2.7 dB, while in measurements, this value was around 1 dB. This can be explained because the manufacturer does not provide

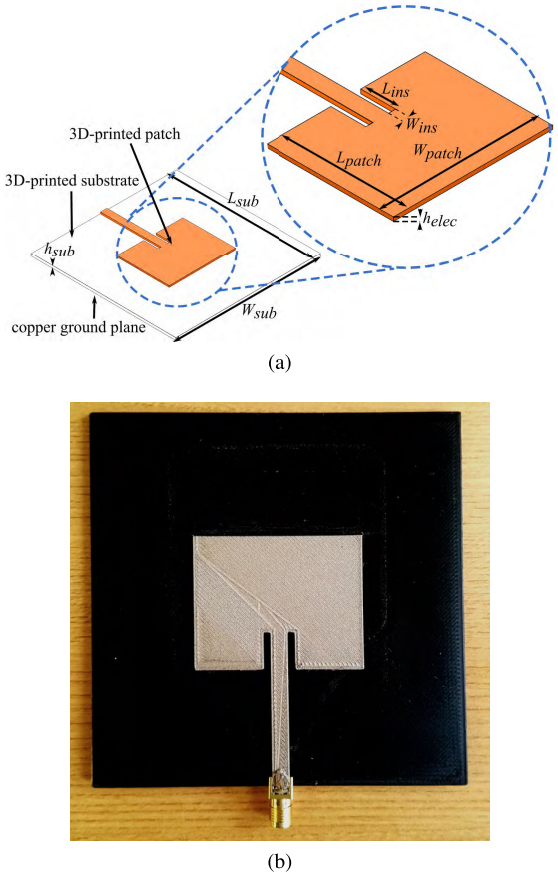

FIGURE 11. Microstrip 3D-printed patch antenna. a) Isometric layout. b) Top view of the constructed microstrip patch antenna.

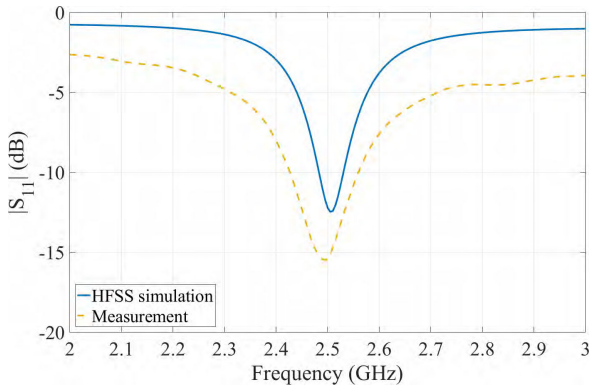

FIGURE 12. Simulated and measured reflection coefficient $|S_{11}|$ as a function of frequency of the microstrip 3D-printed patch antenna.

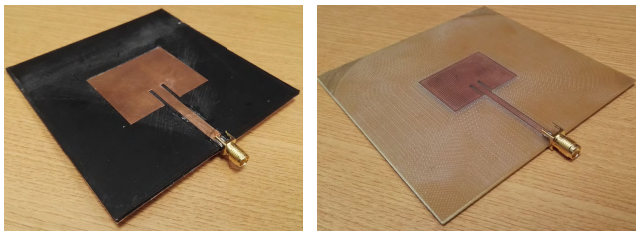

(a) (b)

FIGURE 13. Constructed patch antennas for comparison. a) Copper foils over PLA. b) Copper etched over FR-4.

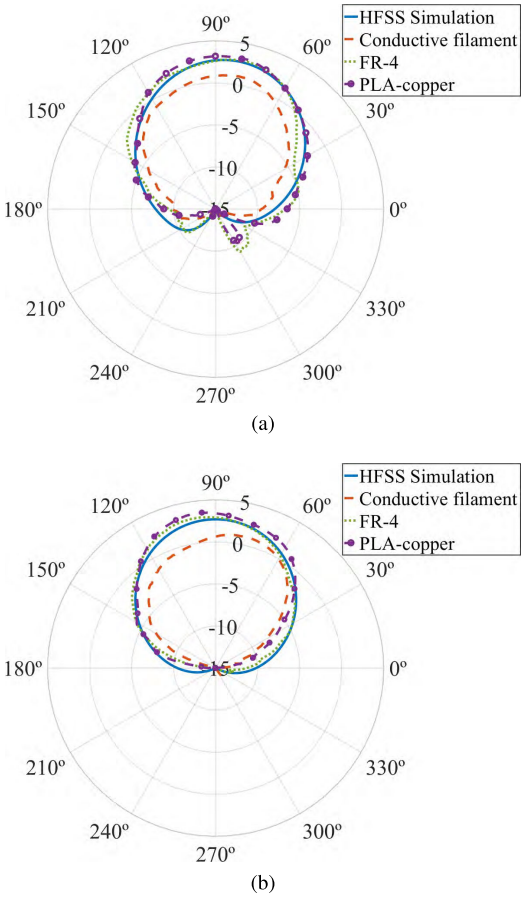

FIGURE 14. Measured and simulated gain for the 3D-printed patch antenna with conductive filament and compared with two reference antennas at the resonant frequency f_0 a) E-Plane. b) H-Plane.

information regarding conductivity for high frequency, and therefore, conductive or dielectric losses are higher than the nominal specified value. In comparison with the reference antennas, we can see that both constructed antennas are very similar in terms of maximum gain (around 3 dB) and confirming the similarities in terms of dielectric losses between both substrates.

B. 3D-PRINTED PYRAMIDAL HORN ANTENNA

The other constructed antenna was a pyramidal horn antenna. This is a widely used antenna topology that has been assessed in previous works using 3D printing [13], [19], [20], [42]–[44]. The difference in the present work is that the antenna was constructed using the least possible amount of conductive filament, and its radiation characteristics were measured to compare them with an identical simulated antenna made by perfect conductor (PEC) layers and with a horn antenna simulated with the electrifi parameters.

For this design, the antenna was conceived to radiate in the C-Band, with a gain of around 15 dB at 5.8 GHz, and fed with a standard WR159 waveguide with a 50 Ω SMA transition. This frequency for this antenna was chosen for two main reasons: the first is that this frequency band is used for vehicle communications [45], and the second is to compare the losses in a different topology, known to have less losses than the microstrip [38]. A layout of the designed antenna is shown in Fig. 15. The final dimensions for the design parameters are $l_{feed} = 9.4$ mm, $l_{wg} = 41.7$ mm, $a_{wg} = 40.38$ mm, $b_{wg} = 20.19$ mm, $R_{ap} = 82.8$ mm, $L_{ap} = 82.8$ mm, $W_{ap} = 121$ mm and $h_{ap} = 91.4$ mm.

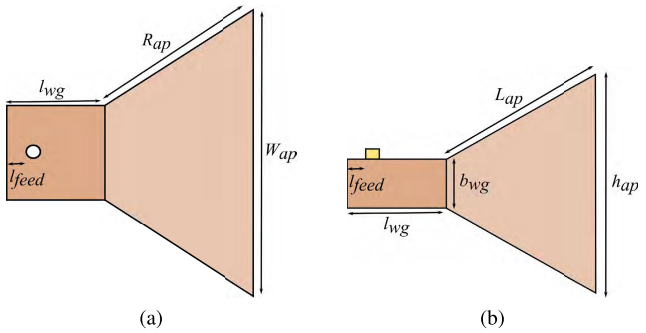

FIGURE 15. Layout of the 3D-printed pyramidal horn. a) Top view. b) Side view.

Regarding the construction of the antenna, it was printed using a concentric infill pattern, with walls of a width of 1 mm, divided in 0.2-mm height layers, and an infill percentage of only 10%. The combination of these parameters provides a constructed antenna that has a total weight (aperture plus feeding) of only 27 grams. This antenna has very low weight compared to a metal-based antenna with similar characteristics, with values of around 750 to 800 grams [46]. In terms of the 3D printing process, the horn can be printed without any supporting structure because of the angles obtained for the horn aperture are lower than the critical angle that the printer can print without a support structure for this material. Therefore the printing process was a normal additive process layer-over-layer. In Fig. 16 is shown the structure of the horn antenna on the CURA software before printing. The 3D-printed pyramidal horn antenna is shown in Fig. 17.

The gain radiation pattern of the antenna at 5.8 GHz was measured in an anechoic chamber (Fig. 18), and its results are presented in Fig. 19. The measured results are compared with two HFSS simulated result obtained using the same designed horn antenna but using a perfect electric conductor (PEC) on the walls and other comparison using the Electrifi conductive

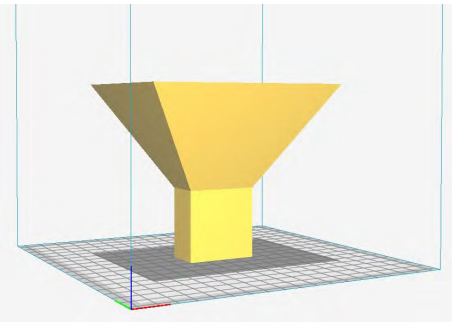

FIGURE 16. Pyramidal horn view on CURA software.

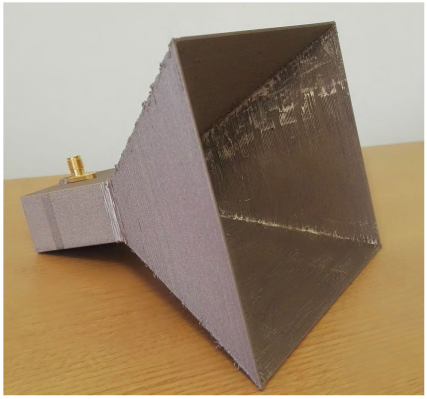

FIGURE 17. 3D-printed pyramidal horn.

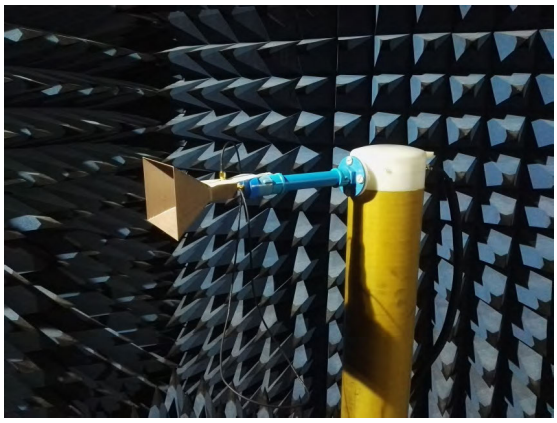

FIGURE 18. 3D-printed pyramidal horn in the anechoic chamber.

filament parameters on the walls. From Fig. 19a (E-plane) and Fig. 19b (H-plane), we can see that we had good agreement between the simulations (both PEC and Electrifi) and measurement in both planes, having very similar maximum gains (around 15 dB on simulation and 14.3 dB on measurement). This can be explained because, in this kind of waveguide topology, the losses are lower than for a resonant topology such as the microstrip patch antenna due to the lower currents [38], [47], [48].

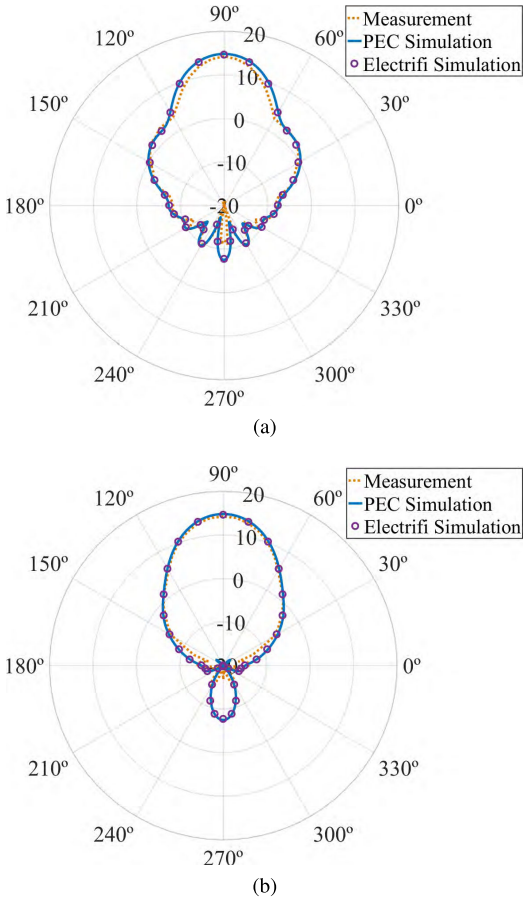

FIGURE 19. Radiation pattern for simulated (PEC), simulated (electrifi) and measured (electrifi) 3D-printed pyramidal horn antenna at 5.8 GHz. (a) E-Plane. (b) H-Plane.

V. CONCLUSION

This work presented a wideband parametric study of classical 3D-printing settings for use in printing high-frequency topologies with Electrifi conductive filament. The three studied parameters, infill percentage, infill pattern and layer height, were varied to construct 27 3D-printed microstrip lines. The results show that there is a dependence between the infill percentage and the losses (the lower the infill percentage is, the higher the losses) for frequencies above 4 GHz. In addition, the infill percentage has an influence on how the different infill patterns can be important in terms of losses on the line. The obtained measured results are important in terms of the use of the conductive filament and printing parameters for high-frequency topologies.

Two antennas were also constructed using 3D printing: a microstrip patch antenna and a low-weight pyramidal horn antenna. The microstrip patch antenna exhibited a good radiation pattern in terms of the radiated mode but with higher losses than for the simulated antenna. The low-weight pyramidal horn antenna showed good agreement in comparison with the simulated antenna, showing lower losses than the microstrip antenna. This can be explained by the fact that

the values of currents for waveguide topology tend to be lower than in a resonant topology such as the microstrip patch antenna. As the low-weight horn antenna has a similar behavior to that of its fully metallic equivalent, it can be very useful for applications where weight is an important issue, such as antennas with critical mechanical movements or antennas on unmanned aerial vehicles (UAV).

ACKNOWLEDGMENT

The authors would like to thank the Departament de Electrónica from the Universidad Técnica Federico Santa María, Valparaíso, Chile, and Prof. Oscar Quevedo and Qiao Chen from KTH, Stockholm, Sweden, for the anechoic chamber measurements. The authors would also like to thank Ocular 3D for all the technical support during the printing process.

REFERENCES

[1] E. Macdonald, R. Salas, D. Espalin, M. Perez, E. Aguilera, D. Muse, and R. B. Wicker, "3D printing for the rapid prototyping of structural electronics," *IEEE Access*, vol. 2, pp. 234–242, Dec. 2014.

[2] C. Kim, D. Espalin, M. Liang, H. Xin, A. Cuaron, I. Varela, E. Macdonald, and R. B. Wicker, "3D printed electronics with high performance, multi-layered electrical interconnect," *IEEE Access*, vol. 5, pp. 25286–25294, 2017.

[3] S. Willis, "The maker revolution," *Computer*, vol. 51, no. 3, pp. 62–65, Mar. 2018.

[4] M. Vaezi, H. Seitz, and S. Yang, "A review on 3D micro-additive manufacturing technologies," *Int. J. Adv. Manuf. Technol.*, vol. 67, nos. 5–8, pp. 1721–1754, Jul. 2013.

[5] G. Addamo, O. A. Peverini, M. Lumia, G. Virone, R. Tascone, F. Calignano, and D. Manfredi, "Experimental research activity on additive manufacturing of microwave passive waveguide components," in *Proc. 47th Eur. Microw. Conf. (EuMC)*, Oct. 2017, pp. 496–499.

[6] M. Liang, J. Wu, X. Yu, and H. Xin, "3D printing technology for RF and THz antennas," in *Proc. Int. Symp. Antennas Propag. (ISAP)*, Oct. 2016, pp. 536–537.

[7] A. Périgaud, S. Bila, O. Tantot, N. Delhote, and S. Verdeyme, "3D printing of microwave passive components by different additive manufacturing technologies," in *Proc. IEEE MTT-S Int. Microw. Workshop Ser. Adv. Mater. Process. RF THz Appl. (IMWS-AMP)*, Jul. 2016, pp. 1–4.

[8] L. G. Menéndez, O. S. Kim, F. Persson, M. Nielsen, and O. Breinbjerg, "3D printed 20/30-GHz dual-band offset stepped-reflector antenna," in *Proc. 9th Eur. Conf. Antennas Propag. (EuCAP)*, Apr. 2015, pp. 1–2.

[9] C. M. Shemelya, M. Zemba, M. Liang, D. Espalin, C. Kief, H. Xin, R. B. Wicker, and E. W. MacDonald, "3D printing multi-functionality: Embedded RF antennas and components," in *Proc. 9th Eur. Conf. Antennas Propag. (EuCAP)*, Apr. 2015, pp. 1–5.

[10] F. Bongard, M. Gimersky, S. Doherty, X. Aubry, and M. Krummen, "3D-printed Ka-band waveguide array antenna for mobile SATCOM applications," in *Proc. 11th Eur. Conf. Antennas Propag. (EUCAP)*, Mar. 2017, pp. 579–583.

[11] X. Shang, P. Penchev, C. Guo, M. J. Lancaster, S. Dimov, Y. Dong, M. Favre, M. Billod, and E. de Rijk, "*W*-band waveguide filters fabricated by laser micromachining and 3-D printing," *IEEE Trans. Microw. Theory Techn.*, vol. 64, no. 8, pp. 2572–2580, Aug. 2016.

[12] S. Mufti, A. Tennant, and L. Seed, "3D printed electrically small planar inverted-F antenna: Efficiency improvement through voluminous expansion," in *Proc. IEEE Int. Symp. Antennas Propag. (APSURSI)*, Jun./Jul. 2016, pp. 811–812.

[13] E. A. Rojas-Nastrucci, J. Nussbaum, T. M. Weller, and N. B. Crane, "Metallic 3D printed Ka-band pyramidal horn using binder jetting," in *Proc. IEEE MTT-S Latin Amer. Microw. Conf. (LAMC)*, Dec. 2016, pp. 1–3.

[14] Y. Tawk, M. Chahoud, M. Fadous, J. Costantine, and C. G. Christodoulou, "The miniaturization of a partially 3-D printed quadrifilar helix antenna," *IEEE Trans. Antennas Propag.*, vol. 65, no. 10, pp. 5043–5051, Oct. 2017.

[15] K. Johnson, M. Zemba, B. P. Conner, J. Walker, E. Burden, K. Rogers, K. R. Cwiok, E. Macdonald, and P. Cortes, "Digital manufacturing of pathologically-complex 3D printed antennas," *IEEE Access*, vol. 7, pp. 39378–39389, 2019.

[16] Y. Li, C. Wang, H. Yuan, N. Liu, H. Zhao, and X. Li, "A 5G MIMO antenna manufactured by 3-D printing method," *IEEE Antennas Wireless Propag. Lett.*, vol. 16, pp. 657–660, 2017.

[17] R. A. Bahr, Y. Fang, W. Su, B. Tehrani, V. Palazzi, and M. M. Tentzeris, "Novel uniquely 3D printed intricate Voronoi and fractal 3D antennas," in *IEEE MTT-S Int. Microw. Symp. Dig.*, Jun. 2017, pp. 1583–1586.

[18] A. H. Wahyudi, J. T. S. Sumantyo, S. Wijaya, and A. Munir, "PLA-based 3D printed circularly polarized X-band horn array antenna for CP-SAR sensor," in *Proc. Int. Workshop Antenna Technol. (iWAT)*, Mar. 2018, pp. 1–4.

[19] M. van der Vorst and J. Gumpinger, "Applicability of 3D printing techniques for compact Ku-band medium/high-gain antennas," in *Proc. 10th Eur. Conf. Antennas Propag. (EuCAP)*, Apr. 2016, pp. 1–4.

[20] H. Yao, S. Sharma, R. Henderson, S. Ashrafi, and D. MacFarlane, "Ka band 3D printed horn antennas," in *Proc. Texas Symp. Wireless Microw. Circuits Syst. (WMCS)*, Mar. 2017, pp. 1–4.

[21] S. Roy, M. B. Qureshi, S. Asif, and B. D. Braaten, "A model for 3D-printed microstrip transmission lines using conductive electrifi filament," in *Proc. IEEE Int. Symp. Antennas Propag., USNC/URSI Nat. Radio Sci. Meeting*, Jul. 2017, pp. 1099–1100.

[22] I. Piekarz, J. Sorocki, I. Slomian, K. Wincza, and S. Gruszczynski, "Experimental verification of 3D printed low-conductivity graphene-enhanced PLA absorbers for back lobe suppression in aperture-coupled antennas," in *Proc. IEEE-APS Top. Conf. Antennas Propag. Wireless Commun. (APWC)*, Sep. 2018, pp. 780–782.

[23] Y. Li, L. Ge, J. Wang, S. Da, D. Cao, J. Wang, and Y. Liu, "3-D printed high-gain wideband waveguide fed horn antenna arrays for millimeter-wave applications," *IEEE Trans. Antennas Propag.*, vol. 67, no. 5, pp. 2868–2877, May 2019.

[24] M. Mirzaee and S. Noghanian, "3D printed antenna using biocompatible dielectric material and graphene," in *Proc. IEEE Int. Symp. Antennas Propag. USNC/URSI Nat. Radio Sci. Meeting*, Jul. 2017, pp. 2543–2544.

[25] S. Zhang, "Three-dimensional printed millimetre wave dielectric resonator reflectarray," *IET Microw., Antennas Propag.*, vol. 11, no. 14, pp. 2005–2009, 2017.

[26] H. Yi, S.-W. Qu, X. Bai, K. B. Ng, and C. H. Chan, "3D printing millimeter-wave lens with scanning beams," in *Proc. IEEE MTT-S Int. Microw. Workshop Ser. Adv. Mater. Process. RF THz Appl. (IMWS-AMP)*, Jul. 2015, pp. 1–2.

[27] J. Pourahmadazar, S. Sahebghalam, S. A. Aghdam, and M. Nouri, "A millimeter-wave Fresnel zone plate lens design using perforated 3D printing material," in *Proc. IEEE MTT-S Int. Microw. Workshop Ser. Adv. Mater. Process. RF THz Appl. (IMWS-AMP)*, Jul. 2018, pp. 1–3.

[28] *MULTI3D*. Accessed: Apr. 4, 2019. [Online]. Available: https://www.multi3dllc.com/

[29] *Black Magic 3D*. Accessed: Apr. 4, 2019. [Online]. Available: https://www.blackmagic3d.com/

[30] *Proto-Pasta*. Accessed: Apr. 4, 2019. [Online]. Available: https://www.proto-pasta.com/

[31] P. I. Deffenbaugh, R. C. Rumpf, and K. H. Church, "Broadband microwave frequency characterization of 3-D printed materials," *IEEE Trans. Compon., Packag., Manuf. Technol.*, vol. 3, no. 12, pp. 2147–2155, Dec. 2013.

[32] S. Moscato, R. Bahr, T. Le, M. Pasian, M. Bozzi, L. Perregrini, and M. M. Tentzeris, "Infill-dependent 3-D-printed material based on ninjaflex filament for antenna applications," *IEEE Antennas Wireless Propag. Lett.*, vol. 15, pp. 1506–1509, 2016.

[33] E. Hajisaeid, A. F. Dericioglu, and A. Akyurtlu, "All 3-D printed free-space setup for microwave dielectric characterization of materials," *IEEE Trans. Instrum. Meas.*, vol. 67, no. 8, pp. 1877–1886, Aug. 2018.

[34] K. Alhassoon, Y. Malallah, A. Sarnaik, C. Kolwalkar, D. N. Kumar, and A. S. Daryoush, "Broadband and accurate material characterization of 3D manufactured RF structures," in *Proc. IEEE MTT-S Int. Microw. Workshop Ser. Adv. Mater. Process. RF THz Appl. (IMWS-AMP)*, Jul. 2018, pp. 1–3.

[35] *Sakata 3D*. Accessed: Apr. 4, 2019. [Online]. Available: https://sakata3d.com/

[36] Y.-H. Chou, M.-J. Jeng, Y.-H. Lee, and Y.-G. Jan, "Measurement of RF PCB dielectric properties and losses," *Prog. Electromagn. Res. Lett.*, vol. 4, pp. 139–148, Jan. 2008.

[37] T. Edwards, *Foundations for Microstrip Circuit Design*. New York, NY, USA: Wiley, 1992.
[38] D. Pozar, *Microwave Engineering*. New York, NY, USA: Wiley, 2011.
[39] *Ocular 3D*. Accessed: Apr. 9, 2019. [Online]. Available: http://ocular3d.cl/
[40] *E3D*. Accessed: Apr. 9, 2019. [Online]. Available: https://e3d-online.com
[41] *Ultimaker Cura*. Accessed: Apr. 5, 2019. [Online]. Available: https://ultimaker.com/
[42] E. A. Rojas-Nastrucci, J. T. Nussbaum, N. B. Crane, and T. M. Weller, "Ka-band characterization of binder jetting for 3-D printing of metallic rectangular waveguide circuits and antennas," *IEEE Trans. Microw. Theory Techn.*, vol. 65, no. 9, pp. 3099–3108, Sep. 2017.
[43] U. Armendariz, S. Rommel, S. Rodriguez, I. T. Monroy, J. J. V. Olmos, and C. B. Olsen, "Evaluation and performance analysis of 3D printing technique for Ka-band antenna production," in *Proc. 46th Eur. Microw. Conf. (EuMC)*, Oct. 2016, pp. 1259–1262.
[44] Y. Levy, M. Raminfar, E. Levine, and H. Matzner, "A multi-horn antenna produced by a 3D printer," in *Proc. Asia–Pacific Int. Symp. Electromagn. Compat. (APEMC)*, Jun. 2017, pp. 275–277.
[45] M. G. Doone, S. L. Cotton, D. W. Matolak, C. Oestges, S. F. Heaney, and W. G. Scanlon, "Pedestrian-to-vehicle communications in an urban environment: Channel measurements and modeling," *IEEE Trans. Antennas Propag.*, vol. 67, no. 3, pp. 1790–1803, Mar. 2019.
[46] *Pasternack*. Accessed: Apr. 5, 2019. [Online]. Available: https://www.pasternack.com/standard-gain-horn-antennas-category.aspx
[47] E. Pucci, A. U. Zaman, E. Rajo-Iglesias, P.-S. Kildal, and A. Kishk, "Study of Q-factors of ridge and groove gap waveguide resonators," *IET Microw., Antennas Propag.*, vol. 7, no. 11, pp. 900–908, Aug. 2013.
[48] C. Balanis, *Advanced Engineering Electromagnetics*. New York, NY, USA: Wiley, 2012.

FRANCISCO PIZARRO (M'19) received the degree in electronics engineering from the Pontificia Universidad Católica de Valparaíso, Chile, in 2010, the M.Sc. degree in communication engineering from the Politecnico di Torino, Italy, in 2010, and the Ph.D. degree in electromagnetics and high frequency systems, plasma engineering from the Institut Supérieur de l'Aéronautique et de l'Espace, Toulouse, France, in 2014. Since 2014, he has been an Associate Professor with the School of Electrical Engineering, Pontificia Universidad Católica de Valparaíso. His research interests include reconfigurable antennas, metamaterials, and plasma/microwave interaction.

ROLANDO SALAZAR was born in Viña del Mar, Chile, in 1987. He received the degree in electronics engineering from the Pontificia Universidad Católica de Valparaíso (PUCV), Chile, in 2019, where he has been a Research Assistant with the Telecommunications Group, since 2019, collaborating on topics related to 3D-printed high frequency devices using conductive filaments on different RF related projects.

EVA RAJO-IGLESIAS (SM'08) was born in Monforte de Lemos, Spain, in 1972. She received the M.Sc. degree in telecommunication engineering from the University of Vigo, Vigo, Spain, in 1996, and the Ph.D. degree in telecommunication engineering from the University Carlos III of Madrid, Madrid, Spain, in 2002. She was a Teaching Assistant with the University Carlos III of Madrid, from 1997 to 2001. She joined the Polytechnic University of Cartagena, Cartagena, Spain, as a Teaching Assistant, in 2001. She joined the University Carlos III of Madrid, as a Visiting Lecturer, in 2002, where she has been an Associate Professor with the Department of Signal Theory and Communications, since 2004. She has been a Full Professor, since 2018. She visited the Chalmers University of Technology, Gothenburg, Sweden, as a Guest Researcher, from 2004 to 2008, where she has been an Affiliated Professor with the Antenna Group, Signals and Systems Department, from 2009 to 2016. She has coauthored over 70 papers in JCR international journals, and more than 120 papers in international conferences. Her current research interests include microstrip patch antennas and arrays, metamaterials, artificial surfaces and periodic structures, gap waveguide technology, MIMO systems, and optimization methods applied to electromagnetism. She was a recipient of the Loughborough Antennas and Propagation Conference Best Paper Award, in 2007, the Best Poster Award in the field of metamaterial applications in antennas at the Metamaterials Conference, in 2009, the Excellence Award to Young Research Staff at the University Carlos III of Madrid, in 2014, and the Third Place Winner of the Bell Labs Prize, in 2014. She is an Associate Editor of the *IEEE Antennas and Propagation Magazine*, and the IEEE Antennas and Wireless Propagation Letters.

MAURICIO RODRíGUEZ (S'15–M'17–SM'18) received the degree in Ingeniero Civil Electrónico and the M.Sc. degree in electronics engineering from the Universidad Técnica Federico Santa María, Valparaíso, Chile, in 2011, and the Ph.D. degree in electronics engineering from the Universidad Técnica Federico Santa María, Valparaíso, in 2017. Since August 2016, he has been with the Escuela de Ingeniería Eléctrica, Pontificia Universidad Católica de Valparaíso, Valparaíso. His main research interests include RF channel modeling, RF measurement, and microwave system design.

SEBASTIAN FINGERHUTH (M'16) received the bachelor's degree (EEng.) from the Pontificia Universidad Católica de Chile (PUC), in 2003, the degree as a Math and Physics Teacher from PUC, in 2003, and the Ph.D. degree (Dr.-Ing.) in acoustics from RWTH Aachen University, Germany, in 2009. As a Researcher and Engineer, he worked in acoustic, psychoacoustic, vibrations, and noise reduction projects with RWTH Aachen University, Germany. He is currently a Full-time Professor with the School of Electrical Engineering, Pontificia Universidad Católica de Valparaíso. He is working in projects in areas such as acoustics, structural vibration, instrumentation, sensors, and signal processing. He is a member of the German Acoustic Society (DEGA) and the American Society of Acoustics (ASA).

GABRIEL HERMOSILLA was born in Chillan, Chile, in 1982. He received the degree in electronics engineering from the University of La Frontera, Temuco, Chile, in 2007, and the Ph.D. degree in electrical engineering from the University of Chile, Santiago, Chile, in 2012. He is currently an Associate Professor with the School of Electrical Engineering, Pontificia Universidad Católica de Valparaíso (PUCV), Valparaiso, Chile. His main areas of research interests include thermal face recognition, pattern recognition, computer vision, and deep learning.